

Numerical Simulation of Double Cup Extrusion Test Using the Arbitrary Lagrangian Eulerian Formalism

Romain Boman, Roxane Koeune and Jean-Philippe Ponthot

Abstract In this chapter Double Cup Extrusion Test (DCET) is modelled using the finite element method with the help of the Arbitrary Lagrangian Eulerian (ALE) formalism. DCET is a tribological test involving very large deformations which are traditionally dealt with complicated and costly remeshing algorithms. Since the topology of ALE meshes should remain constant throughout the simulation, two very thin layers of auxiliary elements are added to the initial mesh of the billet where the material is expected to flow. This numerical trick is combined with an original and efficient node relocation procedure which allows the model to take into account complex geometries of punches. The presented model is firstly validated for limited punch strokes thanks to a purely Lagrangian simulation. It is then compared with results from the literature. Eventually the general nature and the effectiveness of this numerical strategy is demonstrated by a fully-coupled thermomechanical simulation of thixoforming where the final shape of the billet is compared to experimental measurements.

1 Introduction

The Double Cup Extrusion Test (DCET) is a tribological test dedicated to forging operations. Before the conception of DCET, one of the easiest way to quantify friction for this type of processes was the *ring compression test* (see Male and

R. Boman (✉) · R. Koeune · J.-P. Ponthot

Department of Aerospace and Mechanical Engineering, University of Liege, 1 chemin des Chevreuils, 4000 Liège, Belgium
e-mail: r.boman@ulg.ac.be

R. Koeune
e-mail: r.koeune@gmail.com

J. Ponthot
e-mail: jp.ponthot@ulg.ac.be

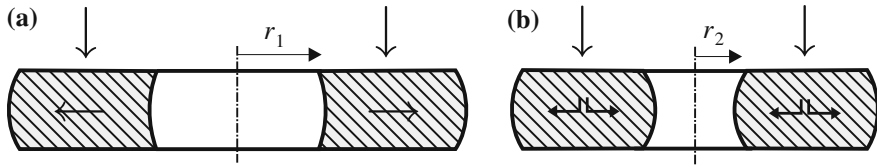


Fig. 1 Schematic description of the ring compression test which may be used to quantify friction in forging operations [25] **a** low friction (good lubrication) **b** high friction (bad lubrication)

Cockcroft [17]), which consists in crushing a flat ring until a prescribed thickness is obtained, as depicted on Fig. 1. If the contacts are well lubricated (Fig. 1a), the material flows outwards and the inner radius of the ring increases. If the friction becomes higher (Fig. 1b), this radial motion is slowed down. A smaller radius is then obtained ($r_2 < r_1$). Consequently, the final inner radius can be used as an indirect measure of friction. However, this simple tribological test reproduces rather badly the real contact conditions and the very high deformations that can be observed at the interfaces between the material and the tools of real forging operations. Indeed, according to Bay [2], it is common to reach pressures close to 2.5 GPa, surface temperatures higher than 600 °C and local surface elongation up to 3000 %. DCET was conceived by Geiger [12] in order to measure friction and to test lubricants in tribological conditions that are closer to these values.

Although DCET is much more elaborated than the ring compression test, the measured friction can still be deduced from very simple geometrical quantities. The experimental setup can be described as follows (see Fig. 2a): a cylindrical billet is placed in a hollow container of same diameter between two punches. During the test, the lower punch is not moving while the upper punch goes down and crushes the specimen. Therefore the material is forced to flow along both punches in such a way that two *cups* are gradually formed. If the contacts were perfectly lubricated, i.e. in the frictionless case, the material would flow symmetrically upwards and downwards. The H-shaped section of the forged billet would have two branches with the same height ($h_1 = h_2$).

In practise, friction is unavoidable and induces a dissymmetry in the process. The obtained final section looks like the one represented in Fig. 2b. The height of the upper cup (h_1) is always higher than the lower one (h_2). The friction can then be quantified by the *cup height ratio* h_1/h_2 . The higher this ratio is, the higher the friction was during the test.

A first direct application to this tribological test is the classification of lubricants according to their respective efficiency in forging conditions. For example, Gariety et al. [11] have compared four lubricants thanks to DCET. They have also studied the possibility of jamming by visualising the grooves on the free surfaces of the billet after the test.

A second interesting application is the numerical estimation of a friction coefficient with the help of the finite element method. In the case of forging, the Tresca's law is usually chosen to model friction:

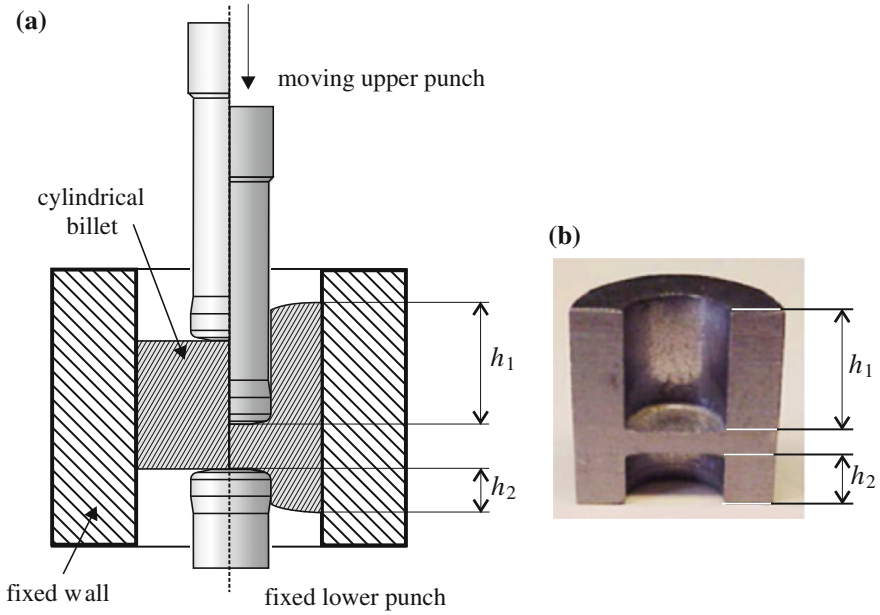


Fig. 2 **a** Principle of the double cup extrusion test from [23]—**b** Picture of a deformed billet after DCET (from Gariety et al. [11])

$$\tau \leq m \tau_{\max} \quad (1)$$

where τ is the friction shear stress at the contact interface, m is the friction coefficient and τ_{\max} is the shear yield stress of the material. A series of numerical simulations of DCET can be performed using a range of friction values m and the corresponding curves of cup height ratios h_1/h_2 versus upper punch displacements can be plotted. This set of calibration curves and the experimental measurement are then used to identify a mean coefficient m for the process [7, 9, 26]. This friction value might be used later, with much care, in more complex numerical simulations of forging which would involve the same material and the same lubricant. The finite element models of the previously cited authors were all using the commercial code DEFORM-2D [24] which conveniently provides an automatic remeshing procedure for quadrangular meshes.

It is important to notice that the relevance of DCET to evaluating friction in forging may be somewhat questionable. In fact, the material flow is mostly influenced by the friction between the billet and the wall of the container. The friction between the punch and the material, which is more representative of a forging operation, plays a less significant role on the dissymmetry of the final shape of the billet. Moreover, some authors, such as Schrader et al. [23], think that the pressures exerted by the billet on the container are not high enough to use a Tresca's law in the finite element models. A Coulomb's law should be more appropriate. Nevertheless, despite these

issues, modelling this tribological test is still very interesting from a numerical point of view.

This chapter is organised in the following way: after a brief review of the ALE formalism, a simplified extrusion model is presented in order to explain the numerical trick that will be used to keep the topology of the ALE mesh constant. Then, this technique is extended to the case of extrusion with curved punches. Next, the model is validated for small punch strokes by comparison with a classical Lagrangian model and a simplistic ALE model using mesh smoothing. For larger punch strokes, the model is compared to results from the literature obtained with a complete remeshing strategy. Finally, a fully-coupled thermomechanical problem of semi-solid forming is described and the final predicted shape of the billet is compared to experimental observations.

This work has been done with Metafor Ponthot [22], an in-house implicit finite element code developed at the University of Liège in Belgium.

2 Overview of the ALE Formalism

In the ALE formalism, unlike in the Lagrangian case which is commonly used in Solid Mechanics, the mesh no longer follows the material motion. Consequently, a new grid coordinate system R_χ is defined and the conservation laws and the constitutive equations are rewritten in terms of the new coordinates χ [3, 4, 8, 22]:

Mass:

$$\left. \frac{\partial \rho}{\partial t} \right|_\chi + \mathbf{c} \cdot \nabla \rho + \rho \nabla \cdot \mathbf{v} = 0 \quad (2)$$

Momentum:

$$\rho \left(\left. \frac{\partial \mathbf{v}}{\partial t} \right|_\chi + (\mathbf{c} \cdot \nabla) \mathbf{v} \right) = \nabla \cdot \boldsymbol{\sigma} + \rho \mathbf{b} \quad (3)$$

Energy:

$$\rho \left(\left. \frac{\partial u}{\partial t} \right|_\chi + \mathbf{c} \cdot \nabla u \right) = \boldsymbol{\sigma} : \mathbf{D} + \rho r + \nabla \cdot \mathbf{q} \quad (4)$$

Material:

$$\left. \frac{\partial \boldsymbol{\sigma}}{\partial t} \right|_\chi + (\mathbf{c} \cdot \nabla) \boldsymbol{\sigma} = \mathcal{H} : \mathbf{D} + \mathbf{W} \boldsymbol{\sigma} - \boldsymbol{\sigma} \mathbf{W} \quad (5)$$

where ρ is the mass density, $\boldsymbol{\sigma}$ is the Cauchy stress tensor, \mathbf{b} and r are the specific body forces and heat sources, u is the specific internal energy, \mathbf{D} and \mathbf{W} are the symmetric and antisymmetric part of the velocity gradient tensor, \mathbf{q} is the heat flux, and \mathcal{H} is a material tensor depending on the constitutive parameters, the stresses,

and the loading history. The last two terms in Eq. (5) result from the particular choice of the Jaumann's objective time derivative.

The convective velocity $\mathbf{c} = \mathbf{v} - \mathbf{v}^*$ is the difference between the material velocity \mathbf{v} and the mesh velocity \mathbf{v}^* . In the case of nonlinear problems, such as metal forming simulations, \mathbf{v}^* should ideally depend on the solution. It is thus an additional unknown of the latter system of equations.

In order to simplify the solution procedure and remain competitive against Lagrangian models, the set of ALE equations is usually solved using an *operator-split* procedure. Each time increment, from time t to $t + \Delta t$, is divided into two successive steps. The first one is performed exactly in the same way as in the classical Lagrangian case. During this *Lagrangian step* the mesh follows the material motion ($\mathbf{v}^* = \mathbf{v}$, $\mathbf{c} = 0$) until an equilibrated configuration is obtained. The second step, also called the *Eulerian step*, is divided into two substeps: the definition of an appropriate mesh velocity \mathbf{v}^* by relocating each node of the mesh to a more suitable position Boman and Ponthot [5], followed by the data transfer from the old mesh configuration to the new one Boman and Ponthot [6]. This transfer involves the Gauss-point values (stress tensor components, history variables of the material such as the equivalent plastic strain) as well as nodal values (velocities, accelerations and temperature).

In the case of simulations of tribological tests such as DCET, the computation of friction forces is obviously very important. Nevertheless this evaluation is not as easy as in the Lagrangian case for which the position of each node of the mesh corresponds to the same material particle during the whole simulation. The following strategy is thus implemented: during the Lagrangian step, a classical penalty method is used to compute the friction occurring at the nodes in contact with a tool. Then, after the Eulerian step, the equilibrated internal forces are recomputed from the transferred stress field on the new mesh. The friction forces are calculated by projection onto the tools and the tangential gaps are recovered from these updated forces.

3 Basic ALE Model of Extrusion

The extrusion process, or more precisely wiredrawing, was first investigated using the ALE formalism by Huétink et al. [15] in 1990. In that early work, the studied problem was 2D axisymmetric, the mesh was purely Eulerian and the stationary solution was sought. Later, Van Haaren et al. [27] and Geijselaers and Huétink [13] built an extrusion model in order to analyse their respective novel ALE convection schemes. Similarly the mesh was fixed in space and a transient computation was performed until the stationary state was reached. In those chapters, the analysis of the results is not exhaustive: the plastic strain is solely visualised in order to compare the numerical diffusion of the newly developed advection schemes. In particular, the friction modelling is not discussed at all.

Transient models of extrusion have been also proposed by Atzema and Huétink [1] and by Ponthot [21]. The ALE formalism can be very useful in this context. In these

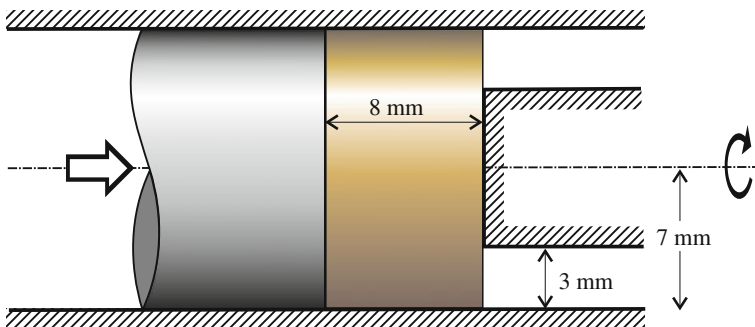


Fig. 3 Axisymmetric geometry of the extrusion model of [21]. A cylindrical specimen is constrained to flow into a *narrow* channel in order to produce a *hollow* cylinder. The specimen shapes at the beginning and the end of the extrusion are completely different

kind of models, the mesh is not Eulerian anymore. Since the ALE formalism requires a constant mesh topology and thus a constant number of finite elements throughout the simulation, it is important to take advantage of the approximate knowledge of the final shape of the extruded billet in order to build the initial mesh. As an illustration of the particular mesh management procedure, Ponthot's model is presented in Fig. 3. The extrusion problem is axisymmetric. A cylindrical billet is pushed by a punch into a narrower channel so that a hollow cylinder is formed. The material is elastoplastic ($E = 200$ GPa, $\nu = 0.3$, $\sigma_Y = 210 + 10 \bar{\epsilon}^P$ MPa) and the friction on the boundaries is modelled by a Coulomb's law with a friction coefficient $\mu = 0.15$.

The transient solution is made up of two quadrangular regions (see Fig. 5): the first region corresponds to the part of the crushed cylindrical billet that still remains between the punches and the second one contains the material which has been already extruded and which lies between the fixed punch and the container wall. At time $t = 0$, the second region should be ideally empty. In order to keep a unique mesh from the beginning to the end of the simulation, Ponthot initially assigns a very small thickness ($h = 0.01$ mm) to this second region and creates a mesh on it. This artificial region is called *auxiliary region* in the remainder of this work. The resulting finite elements of the auxiliary region are thus very flat, but they can *inflate* as a result of the material flux coming from the first region. The node relocation strategy is relatively simple (see Fig. 4). Most of the vertices of the mesh are Lagrangian (i.e. they follow the material motion). Only two vertices are Eulerian (i.e. fixed in space). The line defining the nose of the fixed punch and its neighbour separating both regions of the mesh are also Eulerian. The nodes of the other lines are relocated by defining a cubic spline through them. These splines are then remeshed so that the initial node distribution and their respective curvilinear abscissa are preserved. As far as the inner nodes are concerned, they are continuously relocated thanks to the same transfinite mesher that was used to generate the meshes. These node-relocation methods are fully described in a previous chapter Boman and Ponthot [5].

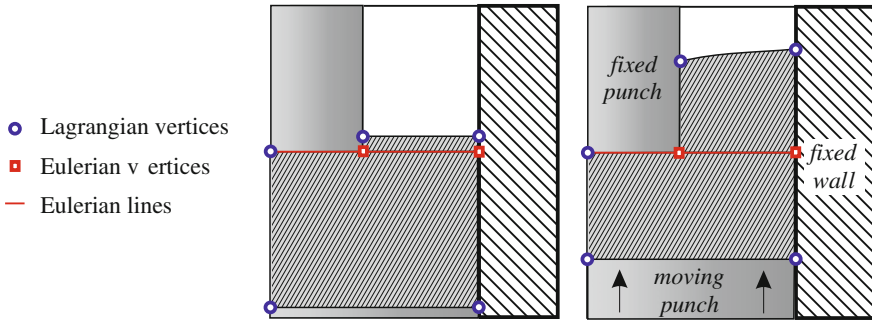


Fig. 4 Node relocation procedure. Thanks to the simple geometry of the fixed punch, the definition of the new mesh is made very easy. The nodes and the line in red are Eulerian. The other lines which have at least one red vertex are remeshed using cubic splines

Figure 5 shows the progress of the simulation. Of course, the proposed mesh management technique entails some issues. First of all, it is mandatory to roughly know the direction of the material flow when setting up the model. Moreover, seeing that the number of finite elements is initially fixed in the auxiliary regions of the mesh, these elements become larger and larger as the simulation progresses and, consequently, the geometry of the extruded parts becomes crudely discretised. Finally, it is not possible to extrude all of the material. The mesh of the billet must always be made up of the same number of elements, but its thickness continuously decreases. The crushed quadrangles, which lie either in the auxiliary region at the beginning of the simulation or in the main region of the mesh at the end of the simulation, lead to some convergence difficulties. On the one hand these finite elements are poorly conditioned for the Lagrangian steps of the ALE algorithm and, on the other hand, the stability criterion of the explicit data-transfer scheme of the Eulerian step is very restrictive concerning the maximum allowable punch displacement during a single time step. As a result, a very small time step has to be used at the beginning and at the end of the simulation (Fig. 6). Figure 7 shows the calculated force on the moving punch during the extrusion operation. The curve obtained by the current implementation is compared to the former results of Ponthot [21]. The trends of both curves are very similar and the final values are identical. The discrepancy between the curves may be explained by the differences in the ALE management of friction.

Despite these limitations, this particular mesh management technique is very attractive for modelling extrusion or any other process for which the material flow is predictable. For example, Gadala et al. [10] used the same ALE method to compute the shape of a metallic chip of a cutting operation.

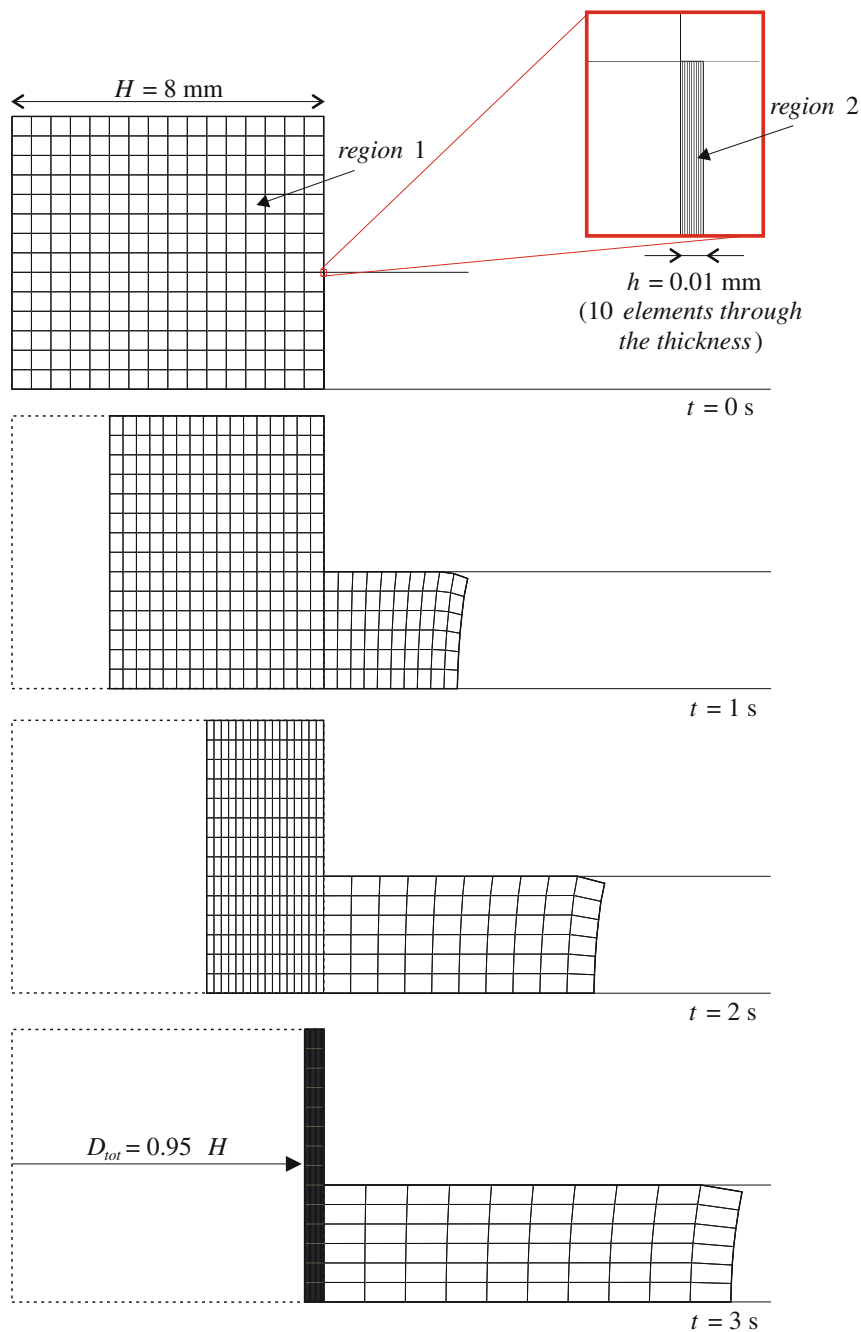


Fig. 5 Results of the extrusion test of Ponthot [21] for a punch stroke up to 95% of the initial thickness of the cylinder (H)

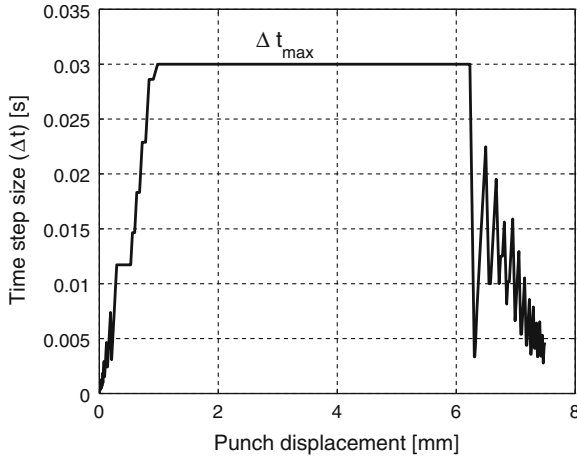


Fig. 6 Size of the time increment Δt along the simulation

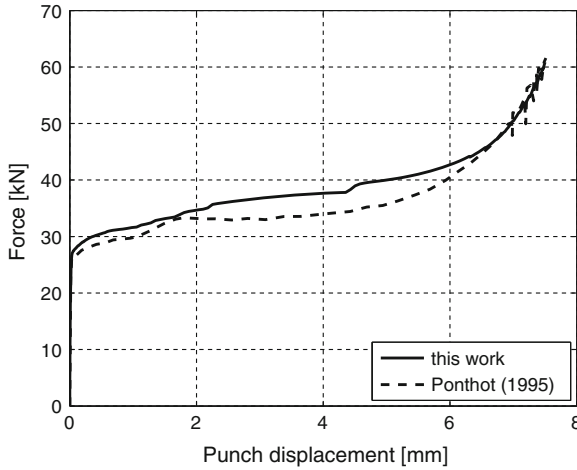


Fig. 7 Extrusion force as a function of the punch displacement and comparison with the results of Ponthot [21]

4 ALE Model of DCET

4.1 Geometry and Parameters

The previous mesh management technique is now applied to a Double Cup Extrusion Test. The chosen geometry was developed at the Engineering Research Center (ERC) of the Ohio State University in order to assess the properties of various lubricants [7]. The exact punch geometry is described in Fig. 8 and the corresponding numerical

Fig. 8 Punch geometry used by Tan et al. [26] and Schrader [23]

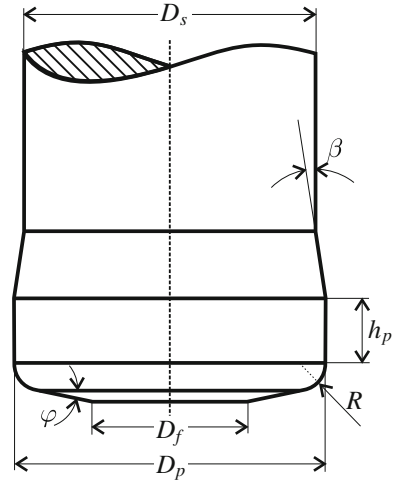


Table 1 Geometry of the extrusion test studied by [23]. The parameters are related to Fig. 8

Punch							Billet	
D_p	D_f	D_s	R	h_p	φ	β	d_0	h_0
[mm]	[mm]	[mm]	[mm]	[mm]	[°]	[°]	[mm]	[mm]
15.88	9.53	15.72	1.17	1.57	10.0	5.0	31.75	31.75

values are listed in Table 1. They are related to the work of [23], which will be the main reference in the remaining part of this chapter. The geometry of the punch is far more complex than the one used by Ponthot. Even if Buschhausen et al. [7] claim that the shape of the punch does not play a significant role on the results (its shape is actually optimised to favour the radial flow of the lubricant, which is not modelled here), this complex shape and all its geometrical details are retained in the model in order to demonstrate the capabilities of our ALE node-relocation algorithm.

The initial diameter of the cylindrical billet d_0 is equal to its height h_0 and to the internal diameter of the container. The *extrusion ratio* is defined as the ratio of the surface of the punch nose and the upper surface of the billet ($r = D_p^2/d_0^2$). This value, deduced from Table 1, is equal to $r = 0.25$. According to Schrader et al. [23], this particular value of r is ideal to observe large variations in the results due to friction conditions.

The material is an AISI 1018 steel with classical elastic properties: Young's modulus $E = 200$ GPa and Poisson's ratio $\nu = 0.3$. The nonlinear hardening is modelled by the following law:

$$\sigma_Y = K (\bar{\epsilon}^P)^n \quad (6)$$

where $K = 735$ MPa and $n = 0.17$. This law has been identified from a standard tensile test the elastic part of which has been neglected. It is employed here in this form, despite the fact that the initial yield stress is zero.

A Tresca's law models the frictional contact: Eq. (1) may be rewritten as $\tau \leq m \sigma_Y / \sqrt{3}$. The extrusion test is supposed to provide the value of this friction coefficient m by identification of an experimental curve and a series of numerical curves obtained with a range of m values. In the following simulations the default value is $m = 0.05$. In practise, the yield stress σ_Y appearing in the Tresca's law is usually chosen as the initial yield stress (see for example the DCET simulations of Tan et al. [26]). In the work of Schrader et al., this numerical value is zero. Consequently, a first possibility is to use the updated local yield stress. However, this value is only defined at the Gauss points of the neighbouring elements of the contact nodes, and not directly at these nodes. The yield stress should thus be extrapolated from the Gauss points to the contact nodes. As a consequence, the friction force evaluated at a given node depends on all the positions of the nodes of the neighbouring elements and a new and more complete stiffness matrix must be computed in order to keep a quadratic convergence rate. The second possibility is to choose a mean value of the yield stress of the material. The cold-drawn AISI 1018 steel is listed on matweb [18] with an initial yield stress of 370 MPa. When this particular value is chosen, numerical results close to the ones of Schrader et al. [23] are obtained. The first choice leads to sensibly different results, which show that some uncertainties remain in the numerical parameters used in the reference work.

The model is axisymmetric and integrated in time by a implicit quasi-static solver (the speed of the punch is about 10 mm/s, which is largely insufficient to produce some inertia phenomena). The mesh is made up of Selective Reduced Integration (SRI) quadrangles. Both punches and the container are assumed rigid. The contact is modelled by the penalty method. The normal and tangent penalty coefficients, p_N and p_T respectively, are determined by trial and error: $p_N = 6 \cdot 10^4$ MPa/mm and $p_T = 6 \cdot 10^3$ MPa/mm for the container wall, and $p_N = 2 \cdot 10^4$ MPa/mm and $p_T = 2 \cdot 10^3$ MPa/mm for the punches. The billet is regularly meshed with elements of 1 mm along the extrusion direction and 0.3 mm along the radial direction for a total of 31×52 elements). As in Ponthot's model presented in the Sect. 4.1, the material flows are anticipated by adding two very thin auxiliary meshes close to both punches (15 elements though the thickness $\varepsilon = 0.2$ mm—see Fig. 10a).

The data-transfer step of the ALE algorithm consists in updating the stresses (pressure p , and deviatoric stress components s_{rr} , s_{rz} , s_{zz}) and the equivalent plastic strain $\bar{\varepsilon}^p$. These five fields are processed by a first-order Godunov scheme [6].

4.2 ALE Mesh Motion

The mesh motion definition is obviously more complex than in the case of the former example. The main difficulty is to define the motion of the red line highlighted in Fig. 9 which represents the surface of the billet under the punch nose and its extension up to the container wall. Unlike its counterpart in Fig. 4, this curve may not be Eulerian because the punch is not stationary anymore. Furthermore, given its slightly convex geometry, the punch is not entirely in contact with the surface of the billet at the

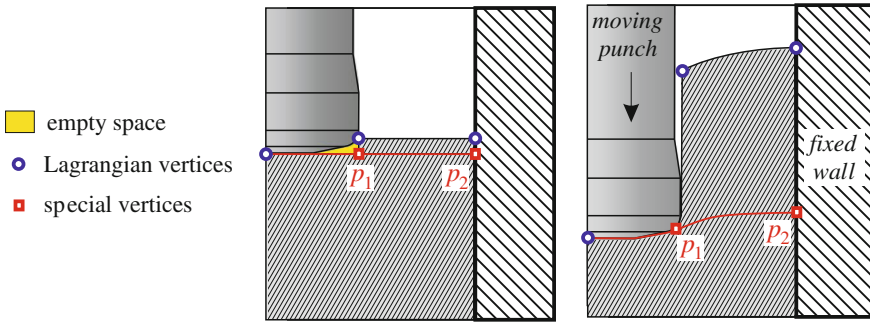


Fig. 9 Node relocation of the DCET model. Unlike the case of Fig. 4, the red line may not be Eulerian anymore

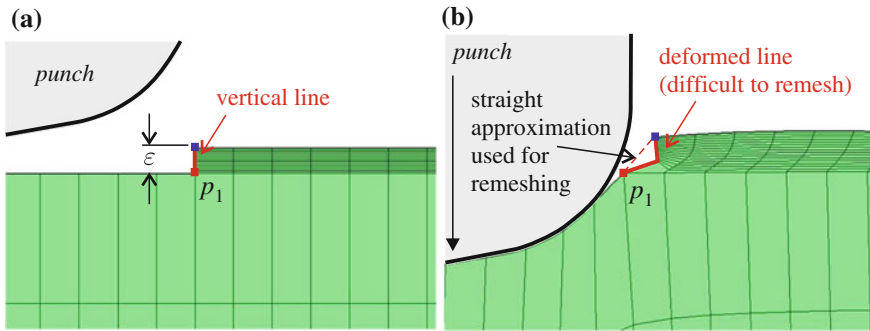


Fig. 10 **a** Zoom on the upper finely-meshed auxiliary region at the beginning of the simulation—**b** Excessive distortion of the elements of the auxiliary domain if the nodes of the red line follow the real motion of the material boundary

beginning of the computation. A small gap, which is initially empty, should be filled during the first moments of the process.

One could imagine to simply prevent the radial motion of node p_1 of Fig. 9. The position of node p_2 would be such that both nodes would have continuously the same Y-coordinate. The other vertices would be Lagrangian. Unfortunately, this solution does not work because an unavoidable material flux is observed between the two regions of the mesh and the thin auxiliary mesh becomes rapidly distorted during the first steps of the simulation. Figures 10a and b explain this issue and the proposed solution. Initially, the vertical line above p_1 is very short and very finely meshed. During the first steps, this line is deformed because the first element of the auxiliary region receives some spurious fluxes related to the relocation of p_1 on the piecewise-linear boundary of the mesh. These fluxes are very small but, compared to the very small area of the elements, they are large enough to highly deteriorate the auxiliary mesh and to make the line impossible to remesh. Consequently this line is remeshed as if it was a straight line until the contact of p_1 with the punch is established.

The simulation is performed in two successive steps. The first one aims at filling up the empty gap between the billet and the punch. At the end of this step, the punch nose is entirely in contact with the billet and the situation becomes similar to the simple extrusion problem of the previous section. During this first step, the radial displacement of node p_1 (Fig. 9) is set to zero and node p_2 is Lagrangian. The vertical line above p_1 is remeshed as if it was straight in order to prevent any distortion problem of the boundary. Doing so, a small inward spurious material flux is tolerated through this boundary.

The second step begins when node p_1 hits the punch surface. At this precise moment, the vertical displacement of node p_2 , as well as those of all the nodes of line (p_1, p_2) , are equaled to the one of p_1 . This line follows thus the vertical motion of the punch. Concerning the former problematic line, it is remeshed at that stage using a cubic spline in order to precisely follow the boundary of the extruded material.

This two-step strategy is symmetrically applied to the lower part of the billet. If some friction is modelled between the billet and the tools, the process is not symmetrical and the transition from the first step to the second does not occur at the same time for the upper and the lower part of the model. This is not a problem in practise.

Finally and more classically, all the remaining curves defining the boundaries of the billet are continuously remeshed using cubic splines. The internal nodes of the main meshed region are relocated thanks to Giuliani's smoothing method Giuliani [14]. This method has been chosen among many others because it produces the most regular mesh in this very case. This iterative smoothing requires five iterations with a overrelaxation coefficient $\omega = 1.5$. Eventually, both auxiliary meshes are continuously remeshed by transfinite mapping.

4.3 Model Validation for Limited Punch Strokes

The ALE model of the previous section is compared with two other models: the first one is a classical Lagrangian model and the second one is an alternative ALE model which simply consists in smoothing the mesh of the billet without defining any auxiliary region. This comparison enables us to validate the proposed ALE node relocation technique.

The punch displacement s (also called *punch stroke*) is limited to 8 mm so that the three models can converge and produce results. Figure 11a shows the Lagrangian solution. The mesh is highly distorted close to the punch nose. Having a closer look at this problematic spot (Fig. 11b), it can be noticed that the mesh boundary highly penetrates the punch. The node-to-surface formulation of the contact with the rigid tool yields erroneous results: the surface of the billet is subjected to very large local elongations and the surface mesh stretches so widely that the curvature of the punch radius is not well described anymore. Since the contact detection only involves the nodes of the boundary, the edges are free to cross the punch analytical surface producing a very large geometrical error.

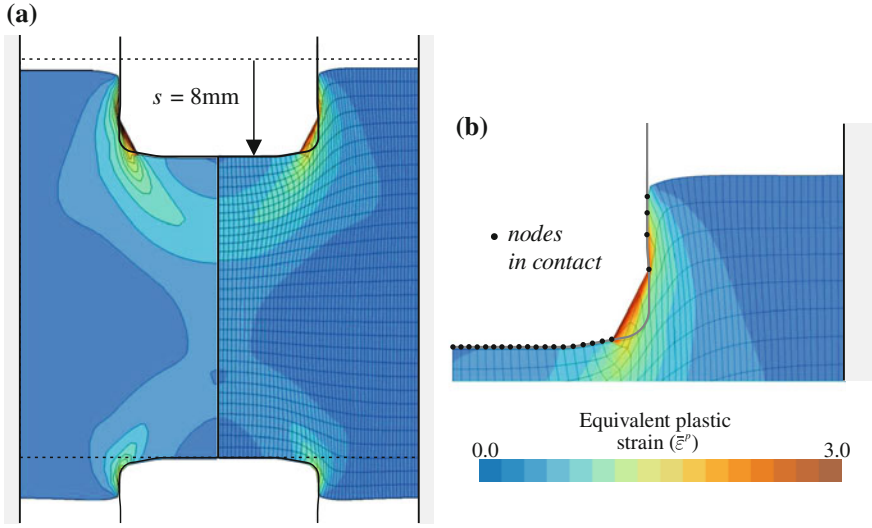


Fig. 11 **a** Lagrangian solution for a 8-mm stroke. These results validate the ALE model for the beginning of the process—**b** Zoom on the Lagrangian solution for which the contact is very badly taken into account

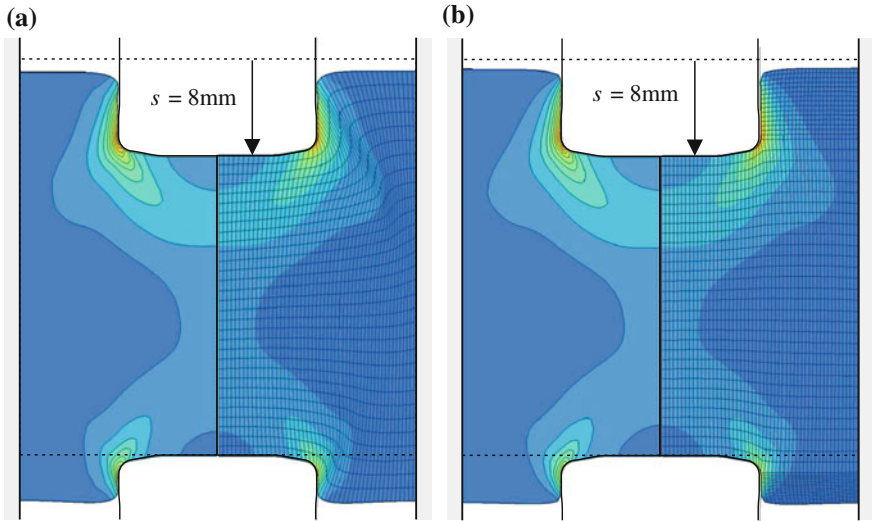


Fig. 12 **a** ALE solution for a 8-mm stroke (simple model). A single region is meshed and a tricky smoothing operator is used—**b** ALE solution for a 8-mm stroke (two-region model)

Figure 12a presents the results obtained by the simple ALE model of DCET without adding any auxiliary meshed regions. The initial mesh is identical to the Lagrangian one. All the boundary nodes are relocated using cubic splines in order

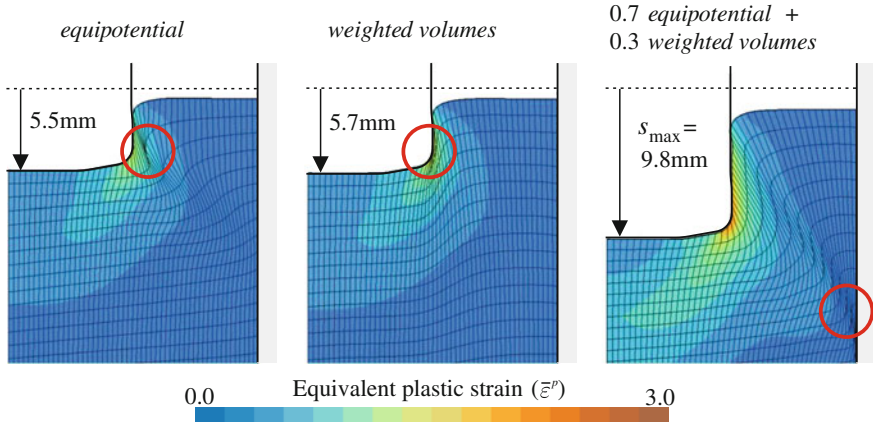


Fig. 13 Comparison of the efficiency of the relocation methods. For each case, the *red circle* indicates the most critical zone of the mesh where the elements are highly distorted

to avoid the excessive stretching of the element edges on the boundary, which was previously discussed. The inner nodes are relocated, after many trials and errors, by a very peculiar combination of two smoothing operators: 70 % of equipotential smoothing and 30 % of weighted volume smoothing Boman and Ponthot [5]. The equipotential part helps to keep the mesh lines almost perpendicular to each other. The weighted-volume part tries to equalise the volumes of the neighbouring quadrangles. Used alone, each of these methods does not permit the computation to converge so far. Figure 13 shows that it is possible to simulate a stroke of $s_{\max} = 5.5$ mm with an equipotential smoother and a stroke of $s_{\max} = 5.7$ mm with a volume-weighted smoother. An appropriate combination of both methods enables the simulation to converge up to 9.8 mm. Nevertheless, these values are much smaller than the experimental stroke value of 27 mm. Even if this stroke could be reached, it is important to notice that the combination factors of the smoothing methods are case-dependant (which means that they are related to a particular value of the friction coefficient m) and very tricky to guess. This simple ALE model is thus useless except for the validation of the two-region ALE model.

Figure 12b shows the results when using the more sophisticated ALE model including the finely meshed auxiliary region for a punch displacement of 8 mm. This time, the quality of the mesh is very good. The equivalent plastic strain distribution is very similar to the one computed by the simple ALE model. Of course, the extruded heights are slightly different because the two-region model starts at $t = t_0$ with nonzero heights ($h_1(t_0) = h_2(t_0) = \varepsilon$). In order to discard this error, the extruded heights are measured without taking into account the initial small heights of the auxiliary meshes (see Fig. 14).

It is possible to compare more precisely these three models. Figure 15 shows the evolution of h_1 and h_2 as a function of the punch stroke. Both ALE models give very close numerical results that follow the trend of the Lagrangian model at the beginning

Fig. 14 Computation of the extruded cup heights h_1 and h_2 in the case of the ALE model using the additional auxiliary meshes. The initial heights ε are subtracted

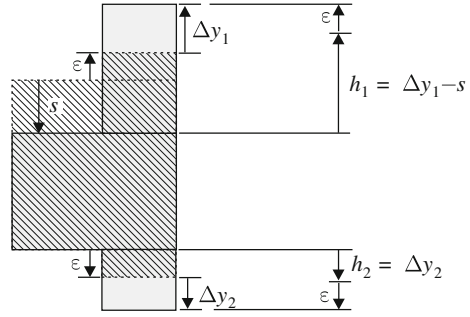
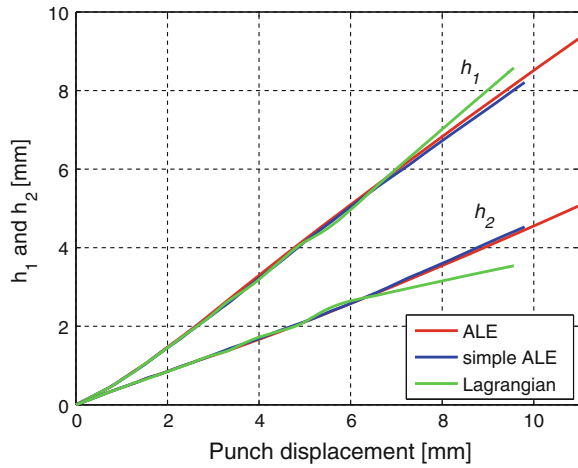


Fig. 15 Comparison of the cup heights h_1 and h_2 for the three models



of the computation. Beyond $s = 5$ mm, the Lagrangian model withdraws from the ALE models because of the penetration of the mesh inside the punch surface (see Fig. 11b). Despite the correction on the computed cup heights, the sophisticated ALE model generates slightly different results from the simple ALE model. This small error ($\Delta h_1 = 0.14$ mm and $\Delta h_2 = -0.08$ mm for $s = 9.8$ mm) certainly comes from the contact length of the billet on the container wall that is not the same in the two cases. The 2-region model is thus subjected to slightly more friction than the simple model. This fact directly affects the corresponding curve of Fig. 16. However, the global trend is quite satisfactory.

In Fig. 17, the curves representing the vertical forces measured on the tools for the three models are very similar at the beginning of the simulation. Starting from $s = 5$ mm, the Lagrangian solution does not model the real process anymore because of the excessive material penetration into the punch. Yet the simple ALE model provides force levels that are very close to the more sophisticated ALE model until it ceases to converge. Finally, as it was expected, the forces of the 3-region ALE model are slightly higher than the ones obtained by the two other models (+1.3 %

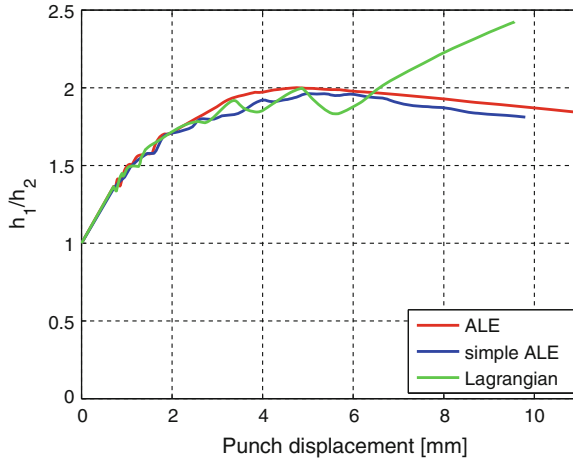


Fig. 16 Comparison of the cup height ratios h_1/h_2 during the process

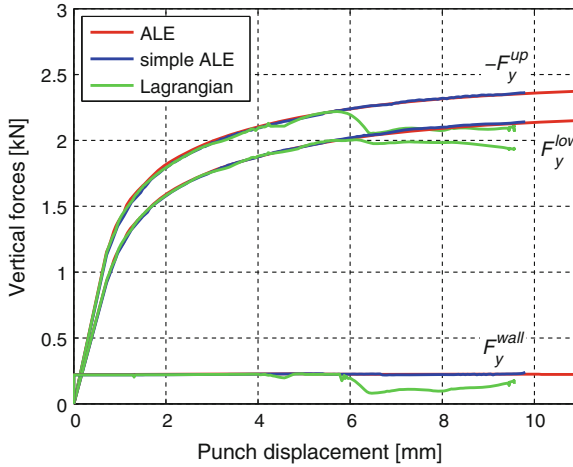


Fig. 17 Vertical forces computed on the *upper* punch F_y^{up} , on the *lower* punch F_y^{low} and on the container wall F_y^{wall} for the three models

for the force on the container wall). This difference, which is barely visible in the Figure, could be further reduced by decreasing the value of ε , at the cost of a slower convergence rate and thus an increase of the total computational time.

This preliminary study proves that the implemented ALE treatment of friction is correct because the same results are obtained independently of the chosen formalism.

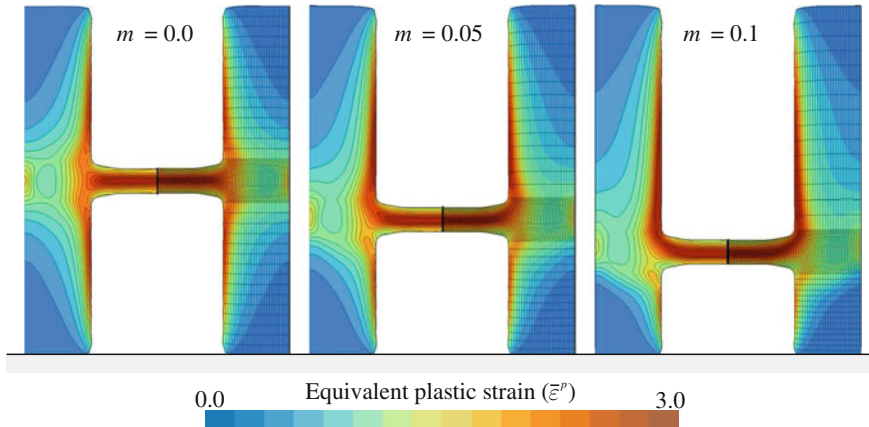


Fig. 18 Deformed billets which have been obtained for several friction values m

4.4 Study of the Whole Process

The whole process is now simulated by using the ALE model until the vertical displacement of the punch reaches $s = 29$ mm, which corresponds to 91 % of the initial height of the billet. When using $m = 0.05$, the problem is solved in 346 time increments corresponding to 422 Newton iterations. The total CPU time is 5'45'' (single-threaded run on an AMD Opteron 254, 8 GHz). This time does not depend much on the value of the friction coefficient m . Approximately half of this time (52 %) is spent in the Lagrangian step of the ALE algorithm. The remaining time splits into node relocation routines (7 %) and the data-transfer scheme (41 %).

The deformed shapes of the billet are presented in Fig. 18 for three values of the friction coefficient m ($m = 0$, $m = 0.05$ et $m = 0.1$). As expected, the upper cup height h_1 becomes larger when the friction coefficient increases. Since the elastic deformations are negligible and thanks to mass conservation, the opposite trend is observed for the lower cup height h_2 . One must keep in mind that this volume conservation is not automatically verified in ALE formalism. A closer look at the volume variation of the mesh reveals that the total volume slightly increases during the ALE computations. Table 2 shows several interesting values: the added volume corresponding to the auxiliary meshes represents about 1 % of the exact initial volume of the experimental billet. At the end of the simulation, an increase of about 0.5 % of the total volume of the mesh is noticed instead of a slight loss of volume that could be intuitively expected from the elastic response of the crushed material. This variation mainly results from the spurious material fluxes that are generated during the remeshing of the boundaries of the mesh. A smaller fraction of this error might also come from the limited accuracy of the data-transfer scheme. Anyways, the observed volume variation of the ALE mesh is always positive and it slightly increases as the friction coefficient m increases.

Table 2 Variation of the volume of the mesh in the ALE simulations of DCET after a punch stroke of 29 mm ($m = 0.05$)

	V [mm ³]	V/V_0 × 100 [%]
Initial volume of the experimental billet V_0	25137	100.00
Added volume (auxiliary meshes)	238	0.95
Initial volume of the model	25375	100.95
Final volume of the model ($m = 0.00$)	25492	101.41
Final volume of the model ($m = 0.05$)	25500	101.44
Final volume of the model ($m = 0.10$)	25525	101.54

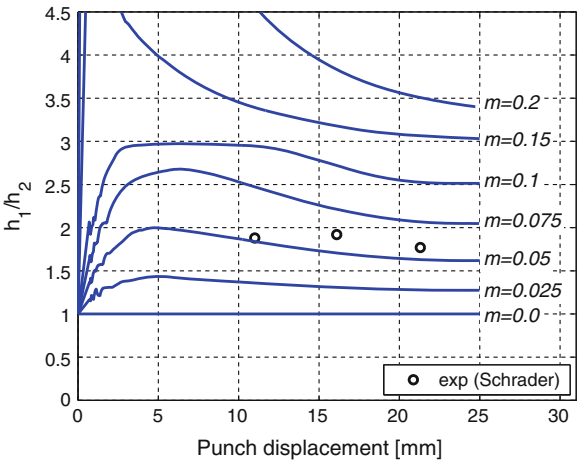


Fig. 19 Set of curves of cup height ratios numerically obtained for a range of friction coefficients m . A value for m may be deduced from the experimental measurements

According to its creator, Geiger [12], the main purpose of DCET is to numerically identify a friction coefficient which is directly related to the chosen lubricant. To reach this goal, a series of simulations are performed by considering a range of friction values m . As an example, Fig. 19 shows the resulting curves in the case of the studied model. The experimental values from Schrader et al. [23]—three punctual measurements—have been superimposed on the numerical curves. A friction value, which is marginally greater than $m = 0.05$, can then be deduced visually from these results.

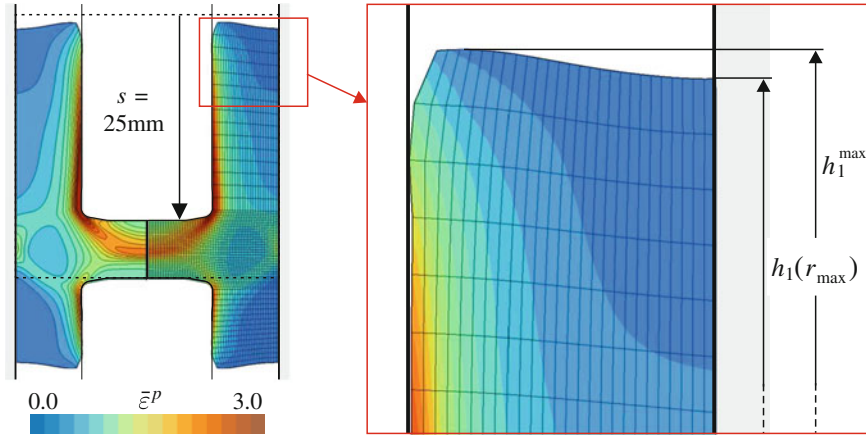


Fig. 20 Two different ways for measuring the height h_1 in the ALE model: either the largest height h_1^{\max} (the measurement position r may vary during the simulation), or the height h_1 measured on the container wall (always at r_{\max}). These simulations correspond to $m = 0.05$ and $n = 0$

4.5 Comparison of Results Obtained by ALE and Remeshing

This section is devoted to a comparison between the ALE model and the numerical and experimental work of Schrader et al. [23]. These authors use DEFORM-2D, a FE code which is dedicated to the simulation of forging and extrusion processes. DEFORM-2D features a sophisticated automatic remeshing algorithm which is very useful to avoid critical distortions of the quadrangular finite elements during the computation. The numerical techniques, which are compared in this section, are thus completely different.

In their work, Schrader et al. study the influence of the hardening coefficient n of the material (see Eq. 6) on the cup height ratio and on the contact pressure when the friction value is $m = 0.05$. The cup height ratio is plotted in Fig. 21 for $n = 0.17$ (the reference value) and $n = 0.0$ (perfectly plastic material). As far as the ALE results are concerned, not one but two curves have been plotted for each hardening coefficient n . The first curve is obtained when the value of h is measured on the container wall (at $r = r_{\max} = d_0/2$). The second one is related to the largest value of h which could be measured at a variable radial position r during the simulation. As an example, Fig. 20 shows the final shape of the billet for a hardening coefficient of $n = 0$. The position of the largest value of h_1 is not located at the container wall. The cup height ratio may vary a lot according to the particular shape of the upper free surface of the material and to the measurement position of h_1 . This is particularly the case when the punch stroke and h are small. For each value of n in Fig. 21, the two ALE curves nicely surround the one obtained by Schrader using DEFORM-2D. For a larger stroke, these three curves converge to an identical final value of the cup height ratio.

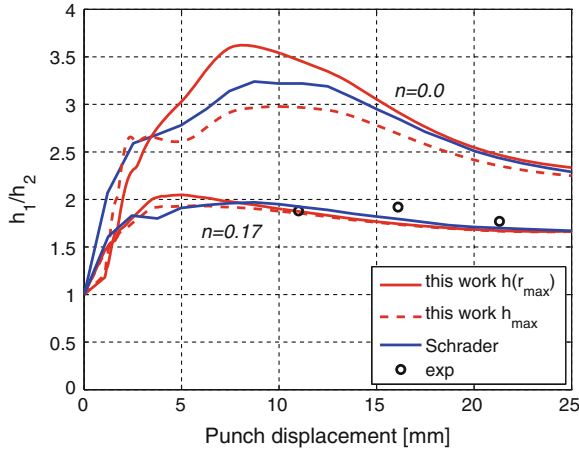


Fig. 21 Influence of the hardening coefficient n of the material on the cup height ratio ($m = 0.05$)

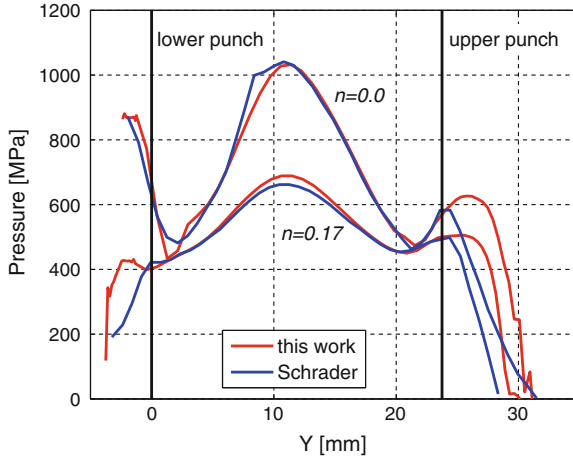
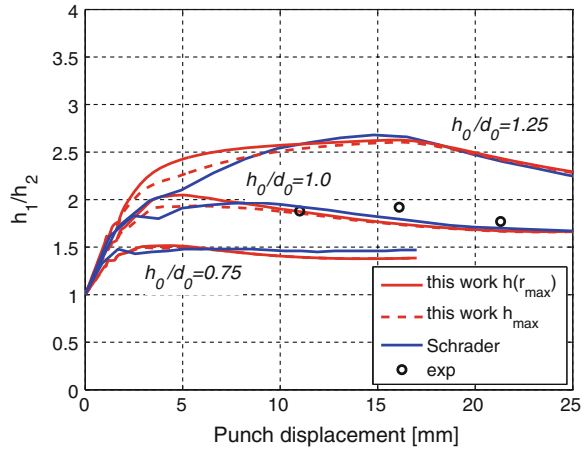


Fig. 22 Pressure field measured on the container wall for a 8-mm stroke and two different values of the hardening coefficient ($m = 0.05$)

The contact pressures on the container wall are plotted in Fig. 22 for a stroke limited to 8 mm and two different materials ($n = 0$ and $n = 0.17$). There is a very good agreement between the results of Schrader et al. and the ALE model. The curves are less close to each other at the level of both punches. Nevertheless, the global shapes of the pressure fields are quite similar.

Schrader et al. also studied the influence of the initial height h_0 of the cylindrical billet on the obtained results. The curves obtained for ratios h_0/d_0 of 0.75, 1.0 (reference value) and 1.25 are presented in Fig. 23. Once again, the ALE results are very close to the published results of Schrader. The largest difference is observed

Fig. 23 Influence of the initial thickness h_0 of the cylindrical billet on the cup height ratio. The friction is kept constant ($m = 0.05$)



for the ratio $h_0/d_0 = 0.75$. In this case, the cup height ratio h_1/h_2 that is computed by the ALE model is a 5 % underestimate of the value computed by DEFORM-2D. Since some assumptions have been made about the supposed treatment of friction and the initial yield stress of the material, this difference may still be considered as rather small. Consequently it can be concluded that the results of the ALE model are consistent with the ones obtained by a remeshing procedure.

5 Application to Thixoforming

In this section, the ALE model of the previous sections is used to simulate a semi-solid forming operation, also known as thixoforming. This kind of process relies on a specific behaviour, called *thixotropy*, of some alloys near their melting temperature. They behave as solids at rest (a billet can sustain its own weight) but they react as liquids during shearing (for example, they can be cut easily).

A thermomechanical constitutive law which models a smooth transition between these two behaviours has been implemented in Metafor [16]. The numerical validation of this law is performed using the ALE model of DCET and the results of a campaign of experimental tests which was conducted at the University of Liège by Pierret, Vaneetveld and Rassili [19, 20] in collaboration with the industrial engineering and mechanical production laboratory of ENSAM (Ecole Nationale Supérieure d'Arts et Métiers, Metz, France).

The adapted numerical model exhibits several additional difficulties compared to the one presented previously: all the material parameters are temperature dependent and a coupled thermomechanical integration scheme is used. The heat transfer between the material (a 100Cr6 steel alloy heated up to 1370 °C) and the rigid tools (initially at 130 °C) is also taken into account. The upper punch velocity, which plays

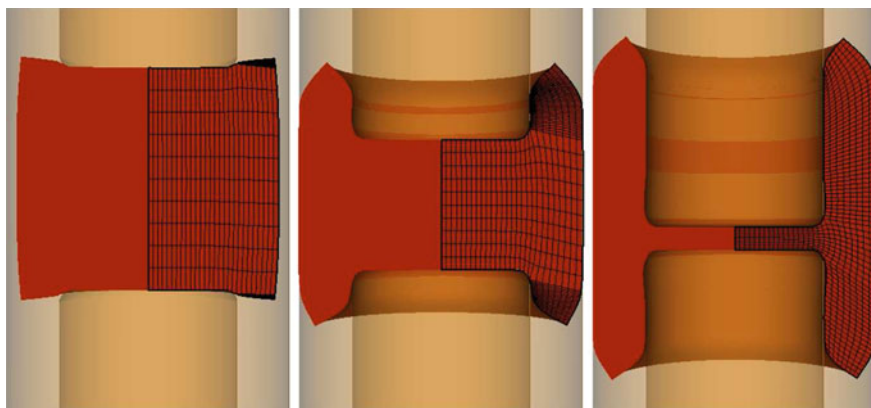


Fig. 24 Illustration of the mesh evolution during the extrusion test

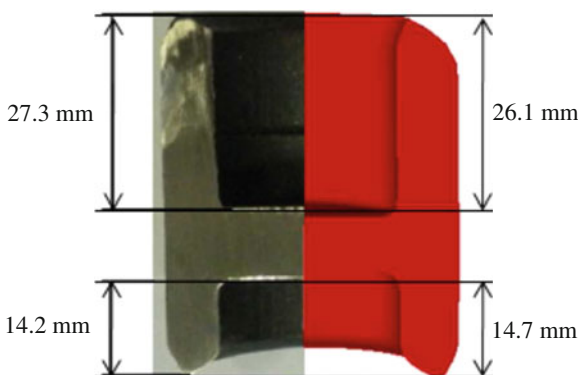


Fig. 25 Comparison of the final shape obtained experimentally (*left*) and the final deformed section resulting from the ALE simulation with a friction coefficient $m = 0.35$ (*right*)

a significant role on the process due to the variable viscosity of the thixotropic material, is not constant. Finally, there is an initial gap between the billet and the container wall at the beginning of the process (see Fig. 24). The filling of this gap requires the definition of an supplementary stage in the time-integration sequence.

Figure 25 presents the final shape of the billet obtained experimentally and numerically. Although the friction coefficient has been chosen to get almost the same cup heights in both cases, it is interesting to see that the simulated upper and lower boundaries of the cups are very similar to the experimental one. This simulation also proves that the mesh management technique presented in this chapter is able to deal with complex material flows.

6 Conclusions

An original 2D model of double cup extrusion test (DCET) has been presented in this chapter. This model efficiently uses the ALE formalism in order to avoid a series of complex and costly remeshing steps during the simulation. Since the DCET is a tribological test, the model is also very interesting to validate the contact treatment on an ALE mesh. An error in the ALE computation of the local friction force would be immediately reflected on the global final shape of the deformed billet.

In order to keep a constant mesh topology, which is a prerequisite condition to use the ALE formalism, it is necessary to add two very thin auxiliary material regions to the initial mesh of the billet. These regions are made up of flat elements which can inflate during the simulation when the billet is crushed between the punches and the material flows from one mesh to the other. Although this particular mesh management technique has been already used by [10, 21], it is the first time that this kind of method is applied to a geometrically-complex process. Indeed, the noses of the punches have not been simplified in the DCET model. They are not planar and their curvature adds a real difficulty to the definition of the mesh motion and the time-integration sequence.

The presented ALE model has been validated by two different means. It has been compared first with an equivalent Lagrangian model during the beginning of the simulations. Secondly, the ALE results have been compared to the ones computed by DEFORM-2D which makes use of an automatic remeshing procedure. A very good agreement has been observed between these two numerical techniques although they are radically different.

Finally, the ALE model of DCET has been used in the frame of a fully-coupled thermomechanical simulation of a semi-solid forming process. Once again, very good results have been obtained without any remeshing operations.

References

1. Atzema EH, Huétink J (1995) Finite element analysis of forward/backward extrusion using ALE techniques. In: Shen Dawson (ed) *Simulation of materials processing: theory, methods and applications* : proceedings of the 5th international conference NUMIFORM. New-York
2. Bay N (1994) The state of the art in cold forging lubrication. *J Mater Process Technol* 46(1–2):19–40. doi:[10.1016/0924-0136\(94\)90100-7](https://doi.org/10.1016/0924-0136(94)90100-7)
3. Benson DJ (1989) An efficient, accurate, simple ale method for nonlinear finite element programs. *Comput Methods Appl Mech Eng* 72(3):305–350. doi:[10.1016/0045-7825\(89\)90003-0](https://doi.org/10.1016/0045-7825(89)90003-0)
4. Benson DJ (1992) Computational methods in lagrangian and eulerian hydrocodes. *Comput Methods Appl Mech Eng* 99(2–3):235–394. doi:[10.1016/0045-7825\(92\)90042-1](https://doi.org/10.1016/0045-7825(92)90042-1)
5. Boman R, Ponthot JP (2012) Efficient ale mesh management for 3d quasi-eulerian problems. *Int J Numer Meth Eng* 92(10):857–890. doi:[10.1002/nme.4361](https://doi.org/10.1002/nme.4361)
6. Boman R, Ponthot JP (2013) Enhanced ALE data transfer strategy for explicit and implicit thermomechanical simulations of high-speed processes. *Int J Numer Meth Eng* 53(0):62–73. doi: <http://dx.doi.org/10.1016/j.ijmpeng.2012.08.007>

7. Buschhausen A, Weinmann K, Lee JY, Altan T (1992) Evaluation of lubrication and friction in cold forging using a double backward-extrusion process. *J Mater Process Technol* 33(1–2):95–108. doi:[10.1016/0924-0136\(92\)90313-H](https://doi.org/10.1016/0924-0136(92)90313-H)
8. Donéa J, Huerta A, Ponthot JP, Rodriguez-Ferran A (2004) Encyclopedia of computational mechanics, chap 14: arbitrary Lagrangian-Eulerian methods, Vol 1. Wiley, pp 413–437. doi:[10.1002/0470091355.ecm009](https://doi.org/10.1002/0470091355.ecm009)
9. Forcelllese A, Gabrielli F, Barcellona A, Micari F (1994) Evaluation of friction in cold metal forming. *J Mater Process Technol* 45(1–4):619–624. doi:[10.1016/0924-0136\(94\)90408-1](https://doi.org/10.1016/0924-0136(94)90408-1)
10. Gadala MS, Movahhedy MR, Wang J (2002) On the mesh motion for ale modeling of metal forming processes. *Finite Elem Anal Des* 38(5):435–459. doi:[10.1016/S0168-874X\(01\)00080-4](https://doi.org/10.1016/S0168-874X(01)00080-4)
11. Gariety M, Ngaile G, Altan T (2007) Evaluation of new cold forging lubricants without zinc phosphate precoat. *Finite Elem Anal Des* 47(3–4):673–681. doi:[10.1016/j.ijmachtools.2006.04.016](https://doi.org/10.1016/j.ijmachtools.2006.04.016)
12. Geiger R (1976) Der stofffluss beim kombinierten napffliesspressen - metal flow in combined can extrusion - (Berichte aus dem Institut für Umformtechnik, Universität Stuttgart). 36, Girardet, Essen, Germany
13. Geijselaers HJM, Huétink J (2000) Semi implicit second order discontinuous Galerkin convection for ALE calculations. In: Onate E, Morgan K, Periaux J, Stein E (eds) (ECCOMAS) European congress on computational methods in applied sciences and engineering, Barcelona
14. Giuliani S (1982) An algorithm for continuous rezoning of the hydrodynamic grid in arbitrary lagrangian-eulerian computer codes. *Nucl Eng Des* 72(2):205–212. doi:[10.1016/0029-5493\(82\)90216-3](https://doi.org/10.1016/0029-5493(82)90216-3)
15. Huétink J, Vreede PT, van der Lugt J (1990) Progress in mixed eulerian-lagrangian finite element simulation of forming processes. *Int J Numer Meth Eng* 30(8):1441–1457. doi:[10.1002/nme.1620300808](https://doi.org/10.1002/nme.1620300808)
16. Koeune R (2011) Semi-solid constitutive modeling for the numerical simulation of thixoforming processes. PhD thesis, University of Liège, Belgium
17. Male AT, Cockcroft MG (1965) A method for the determination of the coefficient of friction of metals under condition of bulk plastic deformation. *J Inst Met* 93:38–46
18. Matweb (2013) Online materials information resource. <http://www.matweb.com/>
19. Pierret J (2009) Quantification de la robustesse du procédé de thixoforgage des aciers. PhD thesis, University of Liège, Belgium.
20. Pierret J, Rassili A, Vaneetveld G, Bigot R, Lecomte-Beckers J (2010) Friction coefficients evaluation for steel thixoforging. *Int J Mater Form* 3:763–766. doi:[10.1007/s12289-010-0882-1](https://doi.org/10.1007/s12289-010-0882-1)
21. Ponthot JP (1995) Advances in Arbitrary Eulerian-Lagrangian finite element simulation of large deformation processes. In: Owen D, Oate E (eds) Computational plasticity: fundamentals and applications -proceedings of the 4th international conference. Pineridge Press Ltd, Barcelona
22. Ponthot JP (1995) Traitement unifié de la mécanique des milieux continus solides en grandes transformations par la méthode des éléments finis. PhD thesis, Université de Liège, Liège, Belgium.
23. Schrader T, Shirgaokar M, Altan T (2007) A critical evaluation of the double cup extrusion test for selection of cold forging lubricants. *J Mater Process Technol* 189(1–3):36–44. doi:[10.1016/j.jmatprotec.2006.11.229](https://doi.org/10.1016/j.jmatprotec.2006.11.229)
24. Scientific Forming Technologies Corporation (2013) DEFORM. <http://www.deform.com/>
25. Sofuoglu H, Rasty J (1999) On the measurement of friction coefficient utilizing the ring compression test. *Tribol Int* 32(6):327–335. doi:[10.1016/S0301-679X\(99\)00055-9](https://doi.org/10.1016/S0301-679X(99)00055-9)
26. Tan X, Bay N, Zhang W (1998) On parameters affecting metal flow and friction in the double cup extrusion test. *Scand J Metall* 27(6):246–252
27. Van Haaren MJ, Stoker HC, van den Boogaard AH, Huétink J (2000) The ALE-method with triangular elements: direct convection of integration point values. *Int J Numer Meth Eng* 49(5):697–720. doi:[10.1002/1097-0207\(20001020\)49:5<697::AID-NME976>3.0.CO;2-U](https://doi.org/10.1002/1097-0207(20001020)49:5<697::AID-NME976>3.0.CO;2-U)

Numerical Simulations of Coupled Problems in
Engineering

Idelsohn, S. (Ed.)

2014, IX, 422 p. 273 illus., Hardcover

ISBN: 978-3-319-06135-1